The Journal of

IMAGING SCIENCE and TECHNOLOGY

# Quantum-Sized Silver, Silver Chloride and Silver Sulfide Clusters

**Gion Calzaferri▲, Dominik Brühwiler, Stephen Glaus, David Schürch, Antonio Currao, and Claudia Leiggener**

*University of Bern, Department of Chemistry and Biochemistry, Bern, Switzerland*

**IS&T**

**The Society for Imaging Science and Technology**

7003 Kilworth Lane, Springfield, VA 22151

703-642-9090; FAX: 703-642-9094

E-mail: info@imaging.org

# Quantum-Sized Silver, Silver Chloride and Silver Sulfide Clusters

**Gion Calzaferri*, Dominik Brühwiler, Stephan Glaus, David Schürch, Antonio Currao, and Claudia Leiggener**

*University of Bern, Department of Chemistry and Biochemistry, Bern, Switzerland*

Thin AgCl layers photocatalytically oxidize water to $O_2$ under appropriate conditions. The photoactivity of AgCl extends from the UV into the visible light region in a process known as self-sensitization, which is due to the formation of silver during the photoreaction. This silver can be almost quantitatively reoxidized electrochemically, making it feasible that a thin AgCl layer deposited on a conducting substrate can be used as a photoanode for water splitting if coupled with an appropriate photocathode. The silver chloride/silver cluster phase boundary plays a decisive role in the photocatalytic silver chloride electrode system. We have therefore studied this interphase by means of quantum chemical calculations from which we report first results, specifically for the $(Ag)_{115}(AgCl)_{192}$ composite. Clusters of semiconducting materials are interesting considering their application as a photocathode in such a device. In this context, we also report the synthesis and properties of luminescent quantum-sized silver sulfide clusters in the cavities of zeolite A. The color of the silver sulfide zeolite A composites ranges from colorless (low loading) to yellow–green (medium loading) to brown (high loading). A low silver sulfide content is characterized by a blue–green luminescence and distinct absorption bands, while samples with medium or high silver sulfide content show an orange or red colored emission and a continuous absorption.

Journal of Imaging Science and Technology 45: 331–339 (2001)

## Introduction

The splitting of water into hydrogen and oxygen driven by solar energy is considered as the "Holy Grail" towards a clean and renewable energy source.[1,2] One of the key problems in the photocatalytic water splitting is the oxidation to oxygen, mainly because of the difficulty in accumulating the necessary four oxidative equivalents required. Our experimental results show that appropriately prepared silver chloride electrodes can fulfill this task. Therefore, we consider this material a suitable choice in a photocatalytic water splitting device. A silver chloride layer acts as a photocatalyst in the presence of a small excess of silver cations with a maximum oxygen evolution rate between pH 4 and 6. Its photoactivity extends from the UV to the visible region due to a process known as self-sensitization. The photocatalytic reaction occurs in two steps. Water is oxidized to oxygen plus protons, and silver cations are reduced to silver upon irradiation. The reduced silver species are reoxidized which makes the system catalytic.[3,4]

$$[n\mathrm{Ag^+}, m\mathrm{AgCl}] + \frac{r}{2}\mathrm{H_2O} \xrightarrow{\text{light}} [(n-r)\mathrm{Ag^+}, m\mathrm{AgCl}, r\mathrm{Ag^0}] + r\mathrm{H^+} + \frac{r}{4}\mathrm{O_2} \quad (1)$$

$$[(n-r)\mathrm{Ag^+}, m\mathrm{AgCl}, r\mathrm{Ag^0}] \xrightarrow{\text{electrode}} [n\mathrm{Ag^+}, m\mathrm{AgCl}] + re^- \quad (2)$$

Equation 1 has been analyzed experimentally[3] and theoretically[5] in some detail. We know that silver cations adsorbed at the surface of silver chloride nanocrystals are necessary for the reaction to proceed. Thus, the light absorption can be considered as a charge transfer excitation from $Cl^-$ to adsorbed $Ag^+$ (see Eq. 3). The electron hole pairs may recombine, or electrons and holes may separate as reduced silver atoms $Ag_{s,i}^0$, and $Cl_s^\bullet$ radicals. The indices $s$ and $i$ refer to surface and interstitial species.

$$[\mathrm{AgCl}]\mathrm{Ag}_s^+ \xrightarrow{\text{light}} [\mathrm{AgCl}]\{\mathrm{Ag^+}, \mathrm{Ag^0}\}_{s,i} + \mathrm{Cl}_s^\bullet \quad (3)$$

The $Cl_s^\bullet$ radicals recombine very fast to form $Cl_2$:

$$2\mathrm{Cl}_s^\bullet \longrightarrow \mathrm{Cl_2} \quad (4)$$

Under the applied conditions (~$10^{-3}$ M $Ag^+$, pH 4–6), the $Cl_2$ reacts with water to produce hypochloric acid. Silver cations act as a catalyst for the decomposition of the latter into molecular oxygen, protons and chloride ions. The chloride ions are bound by the $Ag^+$. These reactions are very fast and we assume that they take place at or very near to the surface.

$$\mathrm{Cl_2} + \mathrm{H_2O} \longrightarrow \mathrm{HOCl} + \mathrm{H^+} + \mathrm{Cl^-} \quad (5)$$

$$2\mathrm{HOCl} \xrightarrow{\mathrm{Ag^+}} \mathrm{O_2} + 2\mathrm{H^+} + 2\mathrm{Cl^-} \quad (6)$$

The reduced silver atoms may react with other silver species ($Ag^0$ atoms, $Ag^+$ ions, or silver clusters) according to Eq. 7, forming positively charged or neutral silver clusters. In its first stages, this reaction is related to the fundamental process of latent image formation in the silver halides. Continuous illumination leads to the formation of printout silver.[6]

Original manuscript received June 5, 2000

*Corresponding author; email: gion.calzaferri@iac.unibe.ch

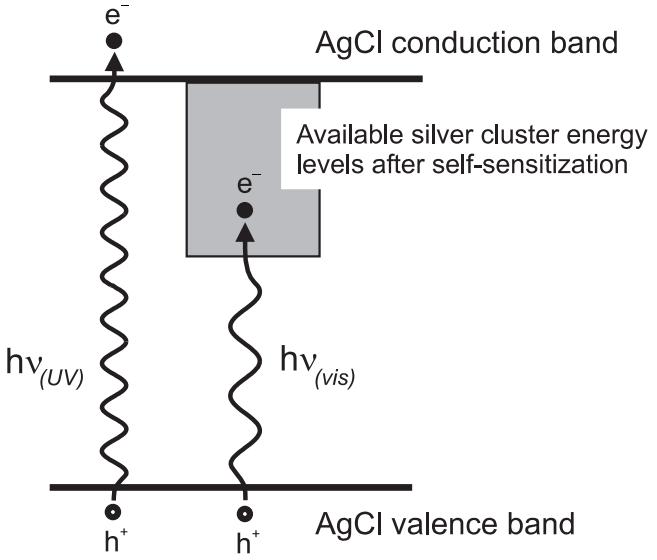


**Figure 1.** Energy level diagram explaining the self-sensitization of silver chloride. The photochemical activity is extended from the near UV into the visible range of the spectrum upon near UV illumination.

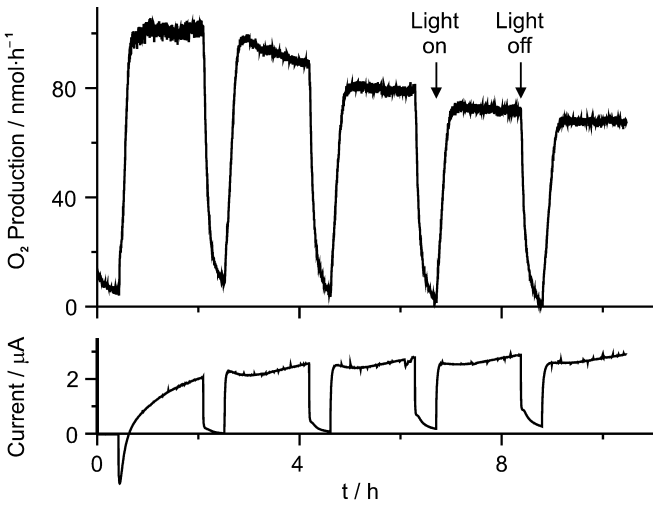


**Figure 2.** Chronoamperometry of a AgCl-coated $SnO_2$:F electrode, carried out at 0.64 V versus NHE, with illumination and dark periods. The $O_2$ production rate (nmol·h$^{-1}$) and the photocurrent (µA; anodic current is drawn upwards) are plotted versus time.[9]

$$Ag^0 + Ag_r^{q+} \rightarrow Ag_{(r+1)}^{q+} \qquad (r \geq 1;\ 0 \leq q \leq r) \qquad (7)$$

The self-sensitization[4,7] of the photochemical activity of AgCl is due to silver clusters adsorbed on its surface. A comparison of the energetic positions of the AgCl[8] band gap and the silver clusters show that the silver clusters have empty energy levels below the conduction band of AgCl (see Fig. 1). In the absence of silver clusters, AgCl does not absorb light below the indirect band gap transition, which is in the near UV at 3.3 eV (≈ 380 nm). Their presence enables a new electronic transition from the AgCl valence band to the empty silver cluster energy levels. The energy for this transition is lower than the energy needed for an optical transition from the AgCl valence band to the AgCl conduction band. Nevertheless, this new optical transition in the visible spectral range still initiates the oxidation of water, because the conduction band is not directly involved in water oxidation. Thus, the photocatalytic oxidation of water on AgCl is extended from the near UV into the visible range of the spectrum. Self-sensitization as observed by us should not be confused with the spectral sensitization effected by silver clusters, also termed photographic Becquerel effect. The latter observation has been attributed to an electron injection from electron-donating silver clusters into the AgCl conduction band.

The reoxidation (Eq. 2) is very simple from a stoichiometric point of view. It is, however, not easy to understand. In order to explain the problem we show in Fig. 2 the results of one of the first successful experiments.[9]

This experiment was carried out with a AgCl-coated electrode produced by precipitation of AgCl on $SnO_2$:F coated glass, in a $10^{-3}$ M silver nitrate solution at pH 4.5. Illumination periods of 100 min duration alternate with dark periods of 25 min duration. It is remarkable that the $O_2$ signal and the photocurrent coincide when the light is switched on and off, which is observed in all experiments. We note that the photocurrent is cathodic (reductive) during the first 12 min of the first illumination period and turns anodic (oxidative) afterwards. About six turnovers with respect to the total amount of AgCl deposited on the electrode (0.46 µmol) were measured before the experiment was stopped after 10.5 h.

The first investigation of the photoelectrochemical properties of AgCl-coated electrodes was made by Becquerel in 1839,[10] a few years after Talbot had realized the first photographic pictures on paper based on AgCl.[11] The photocurrent observed by Becquerel was reductive. An AgCl-coated platinum working electrode and a blank platinum counter electrode were immersed in an aqueous nitric acid electrolyte solution. Illumination of the AgCl-coated electrode by sunlight generated a photovoltage that produced a reductive photocurrent at the AgCl-coated electrode. This is termed the Becquerel effect and represented the first reported photovoltaic device. Equation 2 corresponds to a current of reversed sign with respect to the Becquerel photocurrent. The cathodic current observed during the first 12 min, however, has the same sign as the Becquerel current. Then it changes its behavior and finally corresponds to the anodic current expressed in Eq. 2. We assume that silver clusters formed at the beginning of an experiment do not make electric contact to the conducting glass support. Even nanostructured silver chloride is too good an insulator for electrons, not allowing them to flow to the $SnO_2$:F back contact. However, after some silver clusters have been produced, anodic photocurrents can flow. It was shown that more sophisticated preparation methods for the AgCl layers lead to more stable, more reversible, and more light sensitive electrodes. A typical result obtained on $SnO_2$:F coated glass support with a thin layer of gold, upon which AgCl is prepared by electrochemical oxidation of a 50 nm silver layer, is shown in Fig. 3. The AgCl particle size is smaller than one micrometer (see Ref. 3, Fig. 9). These electrodes display a remarkable stability as evidenced by the sustained $O_2$ production and reoxidation photocurrent. The number of turnovers of AgCl was 11 during the period shown. Obviously much larger turnovers can be achieved by running the experiment over a longer time period. The light intensity from a 450 W Xe arc lamp at the AgCl

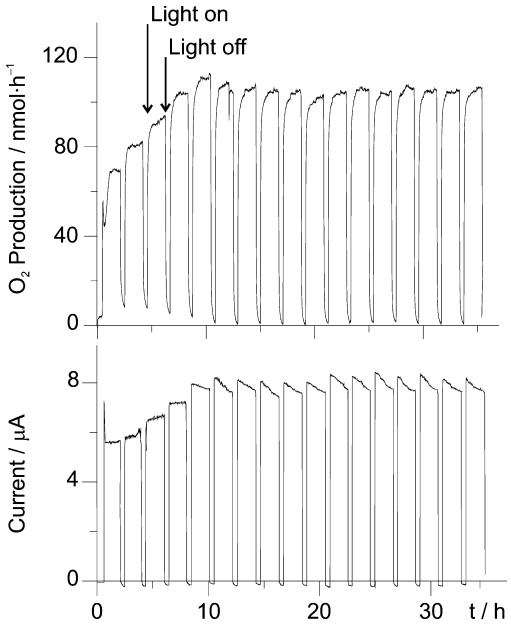


**Figure 3.** Chronoamperometry of an electrochemically prepared AgCl electrode (substrate: $SnO_2$:F coated glass, 1 cm$^2$) modified with a thin gold layer (10 nm), at 0.64 V versus NHE, with illumination and dark periods. The $O_2$ production rate and the photocurrent (anodic current drawn upwards) are plotted versus time.

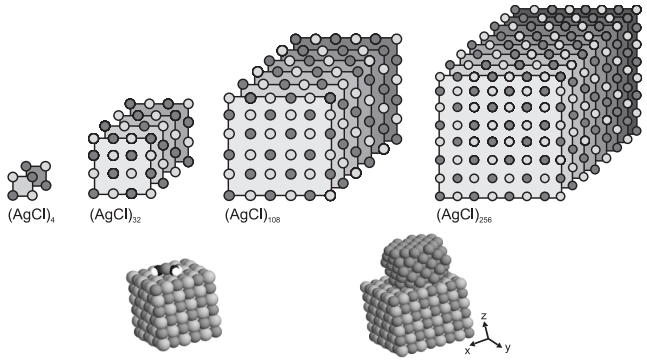


**Figure 4.** Clusters and composites discussed in this article. Top: $(AgCl)_n$ clusters with (100) surfaces. Bottom left: the composite $(Ag)_{115}(AgCl)_{192}$. Bottom right: an adsorbed $Ag^+(H_2O)_2$ on the surface of $(AgCl)_{108}$.

electrode was approximately 50 mW·cm$^{-2}$ of which only part was absorbed.

The silver chloride/silver cluster phase boundary obviously plays a decisive role in the photocatalytic silver chloride electrode system. We have therefore studied this interphase by means of quantum chemical calculations from which we report first results.

Silver sulfide plays an important role in silver halide photography. We also expect it to become important in the processes discussed in this article. We have recently succeeded in preparing the first colored silver sulfide species which luminesce in the visible range of the spectrum.[12] Here we report additional, remarkable characteristics of luminescent quantum-sized silver sulfide clusters in the cavities of zeolite A. A tunable band gap in this semiconductor material makes it very attractive for many purposes, including solar energy conversion.

The oxidation properties of silver chloride photoelectrodes in a photoelectrochemical water splitting system will be discussed in the last section.

## AgCl Surface States and Ag/AgCl Metal-Semiconductor Contact

A deeper theoretical insight of the Ag/AgCl system is important for a better understanding of the photoanodic properties in a water splitting device.[3] This has motivated us to explore selected clusters and composites, which are difficult to investigate experimentally, by theoretical means. We are especially interested in understanding the influence of so called surface states (SURS)[13,14], adsorbed silver ions, and silver clusters on the electronic structure of silver chloride. The metal to silver chloride contact is of special importance with regard to solar cell technology and some first results will be described below. We have recently shown that the EHMO-ASED method[15,16] is well suited for studying the electronic structure of AgCl crystals, AgCl clusters, hydrated silver ions (see Figs. 3 to 6 and Tables III and IV in Ref. 5), as well as for advancing our understanding of silver ions in zeolites.[17] Therefore, this method was applied in the present study.

**AgCl Clusters and Surface States.** It is well established that the (100) surface of AgCl is by far the most stable.[18] For our calculations the $(AgCl)_n$ clusters shown in Fig. 4 were chosen. The AgCl distance increases substantially with increasing size of the cluster (see Fig. 8 in Ref. 5). The change becomes small for larger clusters, for example 0.02 Å from $(AgCl)_{108}$ to $(AgCl)_{256}$. The observed decrease of the HOMO–LUMO gap is exclusively caused by the change of the LUMO position, while the energy of the HOMO remains nearly constant. The latter consists of 3p(Cl) lone pairs, while the LUMO is of 5s(Ag) type. The LUMO is mainly localized at the corner atoms and can therefore be identified as surface state level. These SURS lie about 1 eV below the conduction band edge of the crystal.[5]

Adsorbed $Ag^+(H_2O)_2$ has a marked influence on the electronic structure of silver chloride. The energy level diagram shown in the middle of Fig. 5 represents the situation where the silver ion of $Ag^+(H_2O)_2$ is opposite to a silver atom of a (100) silver chloride surface. The adsorbed silver ion gives rise to a low lying 5s(Ag) level, the energy of which rises quickly when the $Ag^+(H_2O)_2$ is shifted to a position opposite to a chlorine atom on the same surface. The next four higher levels, which are of SURS type, are fully localized on the silver corner atoms. This means that due to the adsorption of a $Ag^+(H_2O)_2$, the charge transfer (CT) properties of silver chloride change. The adsorbed silver ion gives rise to a new energy level which becomes the new LUMO, while the HOMO is not affected.

Main features of the different electronic structures of a AgCl single crystal, a nanocrystal with one $Ag^+(H_2O)_2$ adsorbed and a nanocrystal on which several are adsorbed (some of them already reduced and therefore represented as $(Ag_r^{q+})_{aq}$) are summarized in Fig. 5. Properties of silver clusters and their role in silver halide photography was investigated in detail by Henglein[19] and Belloni.[20] We observed that when a $Ag^+(H_2O)_2$ is placed on all six faces of a $(AgCl)_{108}$ cluster the oscillator strength of the first electronic transition, which is of 5s(Ag) ← 3p(Cl) CT type, rises more than six times with respect to $(AgCl)_{108}$–$Ag^+(H_2O)_2$ due to the coopera-

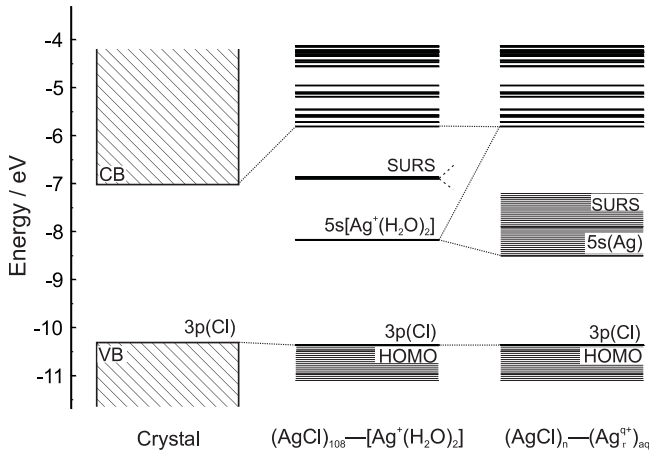


**Figure 5.** Comparison of the electronic structure of a silver chloride crystal, a silver chloride nanocluster with one $Ag^{+}(H_2O)_2$ adsorbed on its surface, and one with several of them adsorbed (some of them already reduced and therefore represented as $(Ag_r^{q+})_{aq}$). The crystal band gap and $(AgCl)_n$–$(Ag_r^{q+})_{aq}$ values correspond to experimental results.

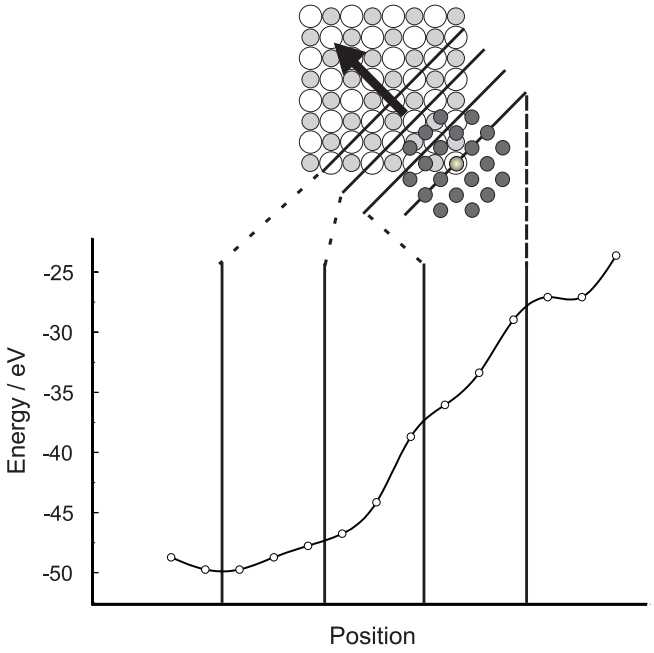


**Figure 6.** Stabilization energy of the Ag/AgCl cluster system. Selected positions are shown.

tion between the adsorbed silver species. It is likely that these CT transitions are responsible for the well-established increased photochemical activity of nanocrystalline AgCl materials in presence of an excess of silver ions.[5]

**Ag/AgCl Metal-Semiconductor Contact.** Band structure diagrams of Schottky and ohmic contacts have been studied in many laboratories.[21,22] Much less is known about the properties of metal/semiconductor interphases on an atomic or molecular level. We are specifically interested in learning more about the influence of adsorbed silver clusters on the electronic states of AgCl. There are a nearly unlimited number of possibilities to create Ag and AgCl cluster models. Silver clusters[23,24] have the tendency to be of spherical shape.[25] We have therefore investigated silver clusters of spherical shape adsorbed on a (1 0 0) silver chloride surface. The $(Ag)_{115}(AgCl)_{192}$ composite illustrated in Fig. 4 was found to be of relevant size for studying important aspects of the electronic structure of such systems. Searching for the most stable position of the $(Ag)_{115}$ on the $(AgCl)_{192}$ we found the result illustrated in Fig. 6. It shows the calculated energy as the cluster is moved along the diagonal line on top of the $(AgCl)_{192}$. The most stable situation is observed when the cluster sits in the central region of this surface. The stabilization is mainly due to favorable interactions between some molecular orbitals of the two adjacent silver and silver chloride layers. Significant exchange of charges takes place at this interface as illustrated in Fig. 7. Three regions are analyzed. The first takes all atoms of the corresponding layer into account (region I). The second excludes the first Ag cluster shell and the corresponding atoms on the AgCl side (region II) and the third excludes the first and the second Ag cluster shell (region III). The overall charges are divided by the number of atoms so that the different regions can be compared. Such an analysis of the electron density along the z axis shows that directly at the junction a negative charge on the AgCl side and a similar positive charge on the Ag side is observed. When comparing with the separated system ($(AgCl)_{192}$ and

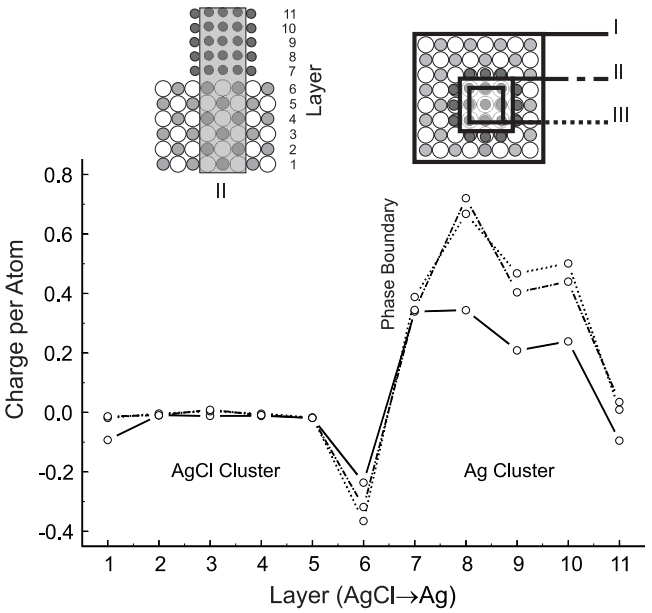


**Figure 7.** Charge per atom in the layers 1 to 11 of the Ag/AgCl cluster system for the regions I (solid), II (dash–dot), III (dot).

$(Ag)_{115}$ at infinite distance), we observe major charge changes on the layers 6, 7, and 8. We also observe a large charge difference at the interface when comparing regions I and II, however the difference between regions II and III is small. The atoms at the surface of the Ag cluster are negatively charged while those inside are positive.

Figure 8 shows the weighted density of states (DOS) of the band gap region of layers 1 to 6. These DOS are similar to the projected DOS in the EHTB (Extended

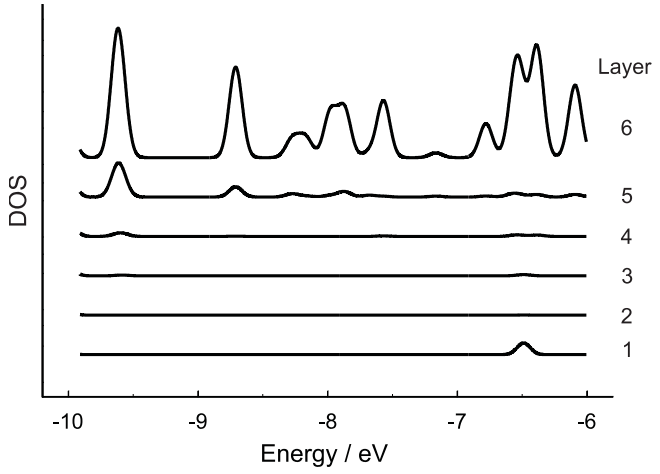


**Figure 8.** Density of states (DOS) observed in the $(Ag)_{115}(AgCl)_{192}$ composite in the band gap region of $(AgCl)_{192}$. The layers 1 to 6 are shown.

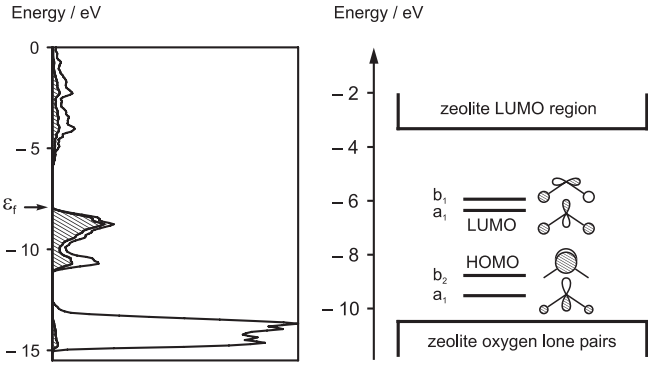


**Figure 9.** Left: Density of states (DOS) plot of α–$Ag_2S$. The hatched region indicates the contribution of sulfur 3p-states (BICON–CEDiT[16] calculation). The Fermi level , is marked by an arrow. Right: HOMO–LUMO region of a hypothetical $Ag_2S$ molecule in comparison to the HOMO–LUMO region of zeolite A (ICON–EDiT[15] calculation).

Hückel Tight Binding) method.[16,26] First, each energy level is weighted with the Mulliken orbital population of the corresponding atoms, then their density is calculated. Details will be described in Ref. 27. The newly formed states lying in the AgCl band gap region, which are induced by the Ag cluster atoms, correspond to what has also been called metal induced gap states (MIGS) in other systems.[28] These states do not penetrate deeply into the silver chloride. They can only be observed in the 5th and 6th layer of the AgCl cluster. Such states should be detectable in specific spectroscopic experiments.

**Quantum Sized Silver Sulfide Clusters**

Bulk silver sulfide has been considered for photoimaging and photodetection in the IR region,[29,30] while molecules and small clusters are known to play an important role in photographic sensitivity.[31–35] In contrast to the thoroughly investigated nanoparticles of semiconductors such as CdS[36] or ZnS[37], only a few studies on clusters of $Ag_2S$ are currently available.[38–42] Silver sulfide nanoparticles show a strong tendency to aggregate into bulk, which renders the preparation of small clusters extremely difficult. By using the well defined cavities of zeolite A, we developed a method of synthesizing silver sulfide clusters in the size regime below 15 Å.[12] The preparation is based on the observation that $Ag^+$ loaded zeolite A can be reversibly activated at room temperature.[17,43] Its reaction with $H_2S$ leads to the formation of silver sulfide clusters inside the zeolite cages. The cluster size can be varied by adjusting the initial amount of exchanged silver ions.

The low temperature phase of bulk silver sulfide (α–$Ag_2S$ or acanthite, stable up to 450 K) is a semiconductor with a monoclinic structure and a band gap of approximately 1 eV at room temperature.[29] The predominant electronic transition in bulk $Ag_2S$ and presumably also in $Ag_2S$ nanoparticles is a charge transfer from 3p(S) to 5s(Ag). Figure 9 shows the calculated DOS of bulk α–$Ag_2S$. The contribution of 3p(S) states to the valence band is much more pronounced than for the conduction band, which is mainly of 5s(Ag) character. An analogous observation can be made for a hypothetical $Ag_2S$ molecule. Furthermore the HOMO–LUMO region of such a molecule, and most probably also of larger silver sulfide clusters, fits well into the energy gap between the oxygen lone pairs of the zeolite A framework and the zeolite A LUMO region, therefore allowing the investigation of its electronic transitions.

In our synthesis of quantum-sized silver sulfide clusters, the zeolite is used as a stabilizing matrix that prevents the silver sulfide particles from growing and aggregating into bulk. The main structural features of zeolite A are the α– and β–cages with diameters of 11.4 and 6.6 Å, respectively (see Fig. 10).[44] It can be assumed that the clusters are located in these cages, with possible interactions between clusters in adjacent cages of high silver sulfide loading.

Silver sulfide clusters were synthesized in sodium zeolite A (NaA) and calcium zeolite A (CaA). The properties of the silver sulfide zeolite A composites depend strongly on the silver sulfide loading density. We have shown that increasing the silver sulfide content leads to the formation of larger clusters and to a drastic variation of the optical absorption and luminescence of the material.[12] The color of the silver sulfide zeolite A composites ($Ag_2S$–NaA-$x$ or $Ag_2S$–CaA-$x$, where $x$ denotes the average number of silver ions per a-cage) ranges from colorless ($0.01 < x < 0.5$) to yellow-green ($0.5 < x < 2$) to brown ($x > 2$). Because pure zeolite A shows no absorption in the investigated spectral range and hydrated $Ag^+$ – loaded zeolite A is colorless as well, it can be concluded that the color of $Ag_2S$–NaA and $Ag_2S$–CaA is caused by the presence of quantum-sized silver sulfide clusters (see Fig. 11).

The silver sulfide zeolite A composites exhibit a variety of luminescence properties depending on the silver sulfide loading density and to a smaller extent, on the co-cations. A low silver sulfide content is basically characterized by a blue–green emission and distinct absorption bands, while samples with medium silver sulfide content show an orange-colored emission and a continuous absorption (see Fig. 12). Further increasing the silver sulfide content ($x > 2$) and therefore the cluster size results in a bathochromic shift of this characteristic emission and a gradual shortening of the luminescence decay times. The decays are multiexponential owing to silver sulfide clusters on different sites inside the zeolite cages and/or a narrow size distribution.

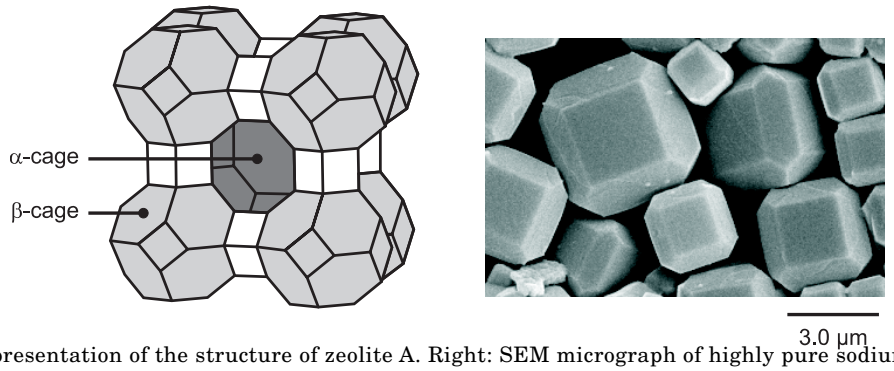


**Figure 10.** Left: Representation of the structure of zeolite A. Right: SEM micrograph of highly pure sodium zeolite A (prepared according to reference 60) used for the synthesis of quantum-sized silver sulfide clusters.

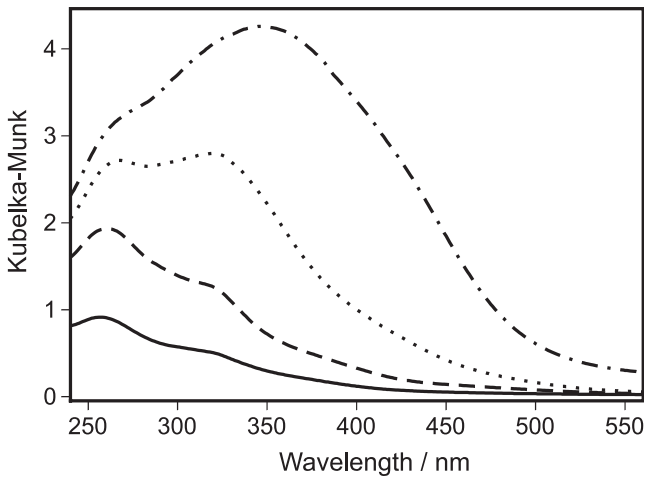


**Figure 11.** Diffuse reflectance spectra of $Ag_2S$–NaA–0.05 (solid), $Ag_2S$–NaA–0.1 (dash), $Ag_2S$–NaA–0.5 (dot) and $Ag_2S$–NaA–2 (dash–dot) under ambient conditions.

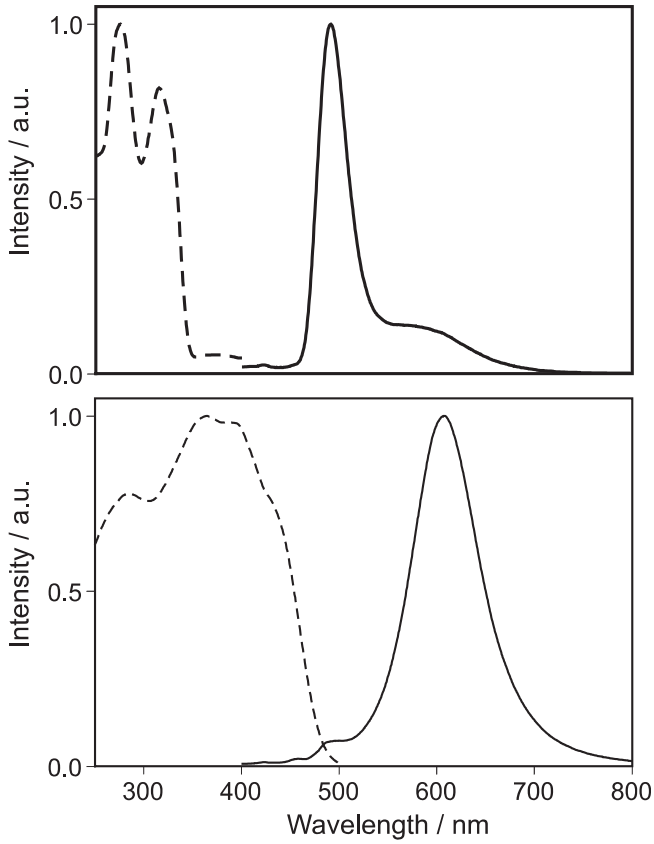


**Figure 12.** Luminescence spectra (solid lines, excitation at 280 nm) and excitation spectra (dashed lines) of $Ag_2S$–CaA–0.01 (top) and $Ag_2S$–CaA–2 (bottom) measured at 80 K.

### Photoelectrochemical Water Splitting with AgCl as Photoanode

Silver chloride is a semiconductor with an indirect band gap of 3.3 to 3.5 eV. The position of the valence band edge can be estimated by means of electrochemical and thermodynamic arguments to be around 2.5 V versus NHE. On the other hand, the energy of the conduction band edges of AgCl and AgBr are nearly equal, namely about –3.3 eV.[45–47] This corresponds to an electrochemical potential of –1.2 V versus NHE (–4.5 eV is equivalent to 0.0 V versus NHE). Adding the value of the band gap energy of AgCl we obtain 2.1 to 2.3 V versus NHE for the position of the valence band edge. Based on these estimates, we will use a value of 2.3 V versus NHE for the position of the valence band edge and –1.0 V versus NHE for the position of the conduction band edge of AgCl (see Fig. 13).

The equilibrium redox potential of a $Ag^+/Ag^0_{bulk}$ silver electrode is 0.62 V versus NHE at a $Ag^+$ concentration of $10^{-3}$ M. As long as all reduced silver species on the AgCl surface build up bulk silver, the value of 0.62 V can be considered to be the lower edge of the silver cluster redox potential range. But if the reduced silver clusters are prevented from forming bulk silver, then the thermodynamic situation is different. We do not know how such a system can be stabilized over an extended period of time. Nevertheless, it is well known that the redox potential of silver clusters $E°[Ag^+/Ag^0_n]$ becomes more negative with decreasing cluster size.[48–50] This is responsible for the decrease of the minimum absorption energy required to excite an electron of the valence band of AgCl, thus extending the photoactivity of the material from the UV to the visible region of the solar spectrum (self-sensitization). Our arguments are therefore based on the equilibrium potential of 0.62 V versus NHE for bulk silver as indicated in Fig. 13.

Silicon has already been used in water splitting devices, in which single or multiple semiconductor p/n

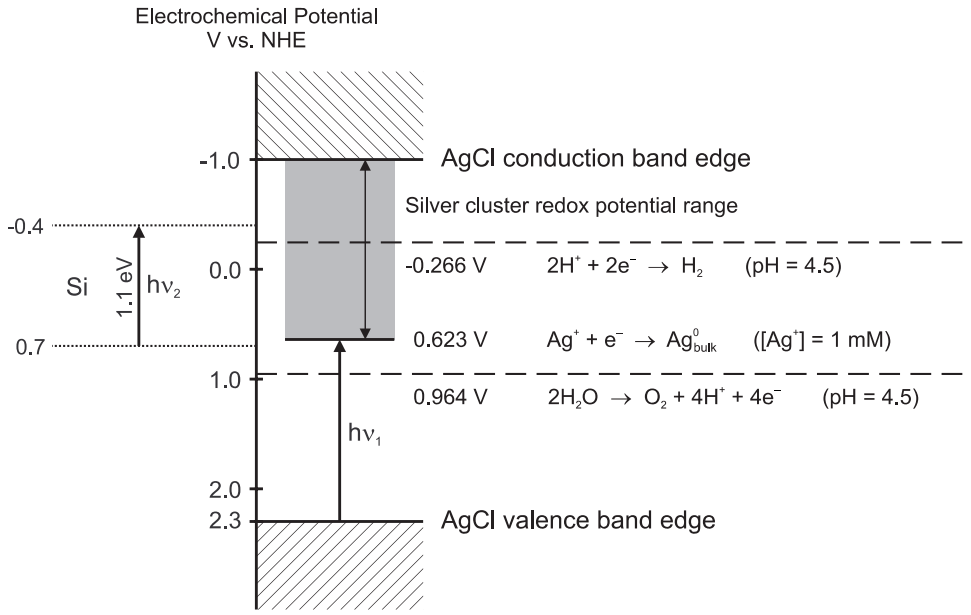


**Figure 13.** Position of the band edges of silver chloride modified with silver species on its surface. On the right side the following redox potentials versus NHE are shown: $Ag^+/Ag^0_{bulk}$ at $[Ag^+] = 10^{-3}$ M, (0.62 V); oxidation ($O_2/H_2O$, 0.96 V) and reduction ($H_2O/H_2$, –0.27 V) of water at pH = 4.5. The electrochemical potential range of silver clusters is represented by the shaded region. On the left side, the position of the valence and conduction band of silicon is shown (band gap 1.1 eV).

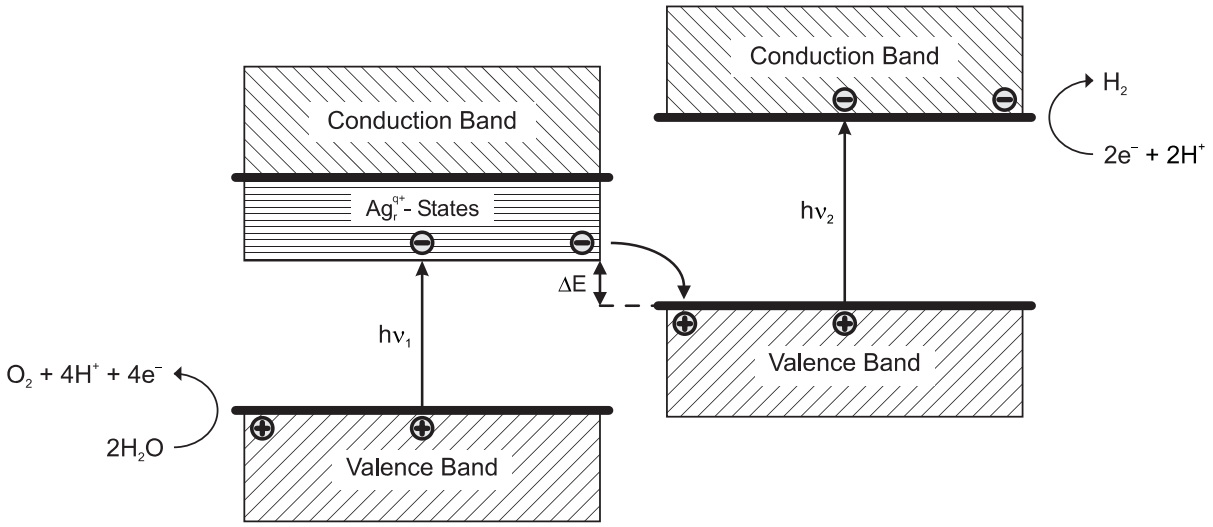


**Figure 14.** Qualitative scheme of a tandem device based on a Ag/AgCl photoanode and an appropriate semiconductor as photocathode.

junctions were utilized as electrodes.[51,52] Another interesting approach for the photoelectrochemical decomposition of water is the use of monolithic tandem cell devices, where different semiconductors layers with different band gaps are connected in series.[53,54] On the left side of Fig. 13 the position of the valence and conduction band edge of silicon is shown (band gap 1.1 eV). The $h\nu_1$ and $h\nu_2$ arrows represent the minimum excitation energies required on each side of a tandem device. To illustrate the energetic requirement for a semiconductor combined with a Ag/AgCl photoanode in a water splitting device, a simplified qualitative scheme of a tandem device is shown in Fig. 14. The main requirement for a suitable photocathode to be combined with a Ag/AgCl photoanode is the following: The valence band edge of the photocathode should have a lower energy than the edge of the silver clusters redox potential range, so that no external bias for the reoxidation of the Ag clusters has to be applied (see $\Delta E$ in Fig. 14).

In Fig. 15 the position of valence band and conduction band edge for a selection of semiconductors is represented.[55–59] The values on the right side are electrochemical potentials relative to three different reference electrodes. On the left side an energy scale in

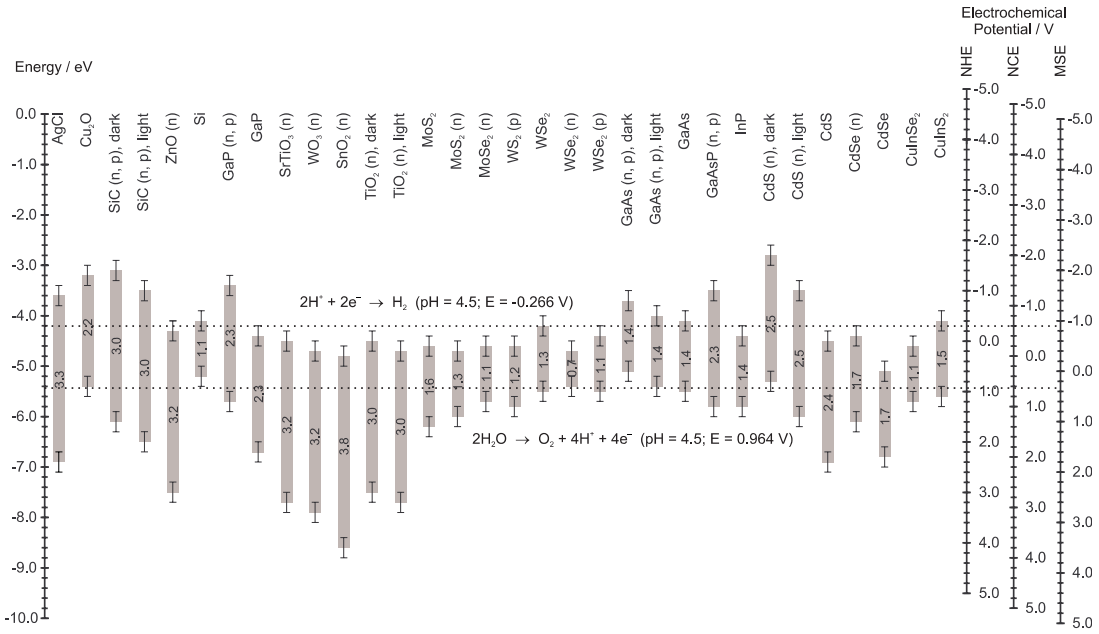


**Figure 15.** The position of valence band and conduction band edges for a selection of semiconductors. A fixed error range of ±0.2 eV was selected for all values. The scales on the right side are electrochemical potentials for three different reference electrodes. NHE: Normal Hydrogen Electrode, $2H^+ + 2e^- \rightarrow H_2$ ($E°$ = 0.000 V); NCE: Normal Calomel Electrode (1M KCl), $Hg_2Cl_2 + 2e^- \rightarrow 2Hg + 2Cl^-$ ($E°$ = 0.280 V versus NHE); MSE: Mercury Sulfate Electrode (Saturated $K_2SO_4$), $Hg_2SO_4 + 2e^- \rightarrow 2Hg + SO_4^{2-}$ ($E°$ = 0.650 V versus NHE). The energy scale on the left side is in eV. See Refs. 55 – 59.

eV was chosen. For some semiconductors different values for the edge positions are reported in the literature, therefore a fixed error range of ±0.2 eV was added.

## Conclusion

AgCl can be used as a photocatalyst for the photoelectrochemical oxidation of water to oxygen. The goal is to combine this half-reaction with a photocatalyst for the reduction of water into hydrogen, to finally get an array capable of water splitting. The amount of $O_2$ produced by the Ag/AgCl system depends on the illuminated surface area of the catalyst. To increase the amount of $O_2$ produced by the Ag/AgCl photoanode, experiments with layers deposited on a structured surface are in progress.

We found that adsorbed $(Ag_r^{q+})_{aq}$ species on the surface of AgCl are responsible for the self-sensitization. The band gap of AgCl decreases substantially by the presence of silver ion 5s states. We also investigated the Ag/AgCl metal-semiconductor contact. The potential energy of a Ag cluster on a AgCl surface is lower compared to a separated system. The boundary between the Ag cluster and the AgCl surface shows predominantly a negative charge on the AgCl side and a positive charge on the Ag side.

Zeolite A is a convenient host material for silver sulfide nanoparticles. The cluster size, and thus the spectroscopic behavior of the silver sulfide clusters can be varied by adjusting the preparation conditions. The silver sulfide zeolite A composites are luminescent in the visible region of the spectrum. The emission ranges from blue, to orange, to red, depending on the size of the clusters.

From the energetic viewpoint many semiconductors seem to be appropriate for use as photocathode together with a Ag/AgCl photoanode in a water splitting device (e.g., $Cu_2O$, Si, SiC, CdS, $Ag_2S$, see also Fig. 15). The main difficulties lie in the stability of the material against photocorrosion and the kinetic requirements to drive the reaction. To test its water splitting capability, the Ag/AgCl photoanode is combined with other semiconductors suitable as a photocathode. Experiments are currently being carried out with an apparatus consisting of two separate compartments connected through a salt bridge. One compartment is used for the Ag/AgCl photoanode and the other for the photocathode.

**Acknowledgment.** We acknowledge financial support by the Schweizerisches Bundesamt für Energiewirtschaft (project no. 36846) and the Schweizerische Nationalfonds (project no. 20-53414.98).

## References

1. G. Calzaferri, D. Brühwiler, S. Glaus, D. Schürch and A. Currao, *Proc. IS&T/SPSTJ's International Symposium on Silver Halide Imaging: Silver Halide in a New Millennium*, IS&T, Springfield, VA, 2000, p. 59.
2. A. J. Bard and M.A. Fox, *Acc. Chem. Res.* **28**, 141 (1995).
3. M. Lanz, D. Schürch and G. Calzaferri, *J. Photochem. Photobiol. A: Chem.* **120**, 105 (1999).
4. K. Pfanner, N. Gfeller and G. Calzaferri, *J. Photochem. Photobiol. A: Chem.* **95**, 175 (1996). Note: The reported quantum efficiencies for $O_2$ evolution are perhaps overestimated. Quantum efficiencies of these systems depend on several parameters. They are currently being reinvestigated in our laboratory under different conditions.
5. S. Glaus and G. Calzaferri, *J. Phys. Chem. B.* **103**, 5622 (1999).
6. T. H. James, *The Theory of the Photographic Process*, 4th ed., Macmillan, New York, 1977.
7. R. Beer, F. Binder and G. Calzaferri, *J. Photochem. Photobiol. A: Chem.* **69,** 67 (1992).
8. S. Sumi, T. Watanabe, A. Fujishima and K. Honda, *Bull. Chem. Soc. Jpn.* **53,** 2742 (1980).
9. M. Lanz and G. Calzaferri, *J. Photochem. Photobiol. A: Chem.* **109**, 87 (1997).
10. E. Becquerel, *C.R. Acad. Sci.* **9**, 561 (1839).
11. L. J. Schaaf, *Out of the Shadows: Herschel, Talbot, and the Invention of Photography*, Yale University Press, New Haven, CT, 1992.
12. D. Brühwiler, R. Seifert and G. Calzaferri, *J. Phys. Chem. B* **103**, 6397 (1999).
13. I. Tamm, *Z. Physik* **76**, 849 (1932).

14. M. Brändle, G. Calzaferri and M. Lanz, *Chem. Phys.* **201**, 141 (1995).
15. R. Rytz, S. Glaus, M. Brändle, D. Brühwiler and G. Calzaferri, ICON–EDiT, Extended Hückel Molecular Orbital and Transition Dipole Moment Calculations, http://iacrs1.unibe.ch, Department of Chemistry and Biochemistry, University of Bern, Freiestrasse 3, 3012 Bern, Switzerland, 2000.
16. M. Brändle, R. Rytz and G. Calzaferri, BICON–CEDiT, Extended Hückel Band Structure and Transition Dipole Moment Calculations, http://iacrs1.unibe.ch, Department of Chemistry and Biochemistry, University of Bern, Freiestrasse 3, 3012 Bern, Switzerland, 2000.
17. R. Seifert, R. Rytz and G. Calzaferri, *J. Phys. Chem. A* **104**, 7473 (2000).
18. S. Karthäuser, in *Proc. IS&T/SPSTJ's International Symposium on Silver Halide Imaging: Silver Halide in a New Millennium*, IS&T, Springfield, VA, 2000, p. 25.
19. A. Henglein, *J. Phys. Chem.* **97**, 5457 (1993).
20. J. Belloni, M. Mostafavi, J. L. Marignier and J. Amblard, *J. Imaging Sci.* **35**, 68 (1991).
21. E. H. Rhoderick and R. H. Williams, *Metal-Semiconductor Contacts*, Oxford Press, Oxford, UK, 1988.
22. P. Würfel, *Physik der Solarzellen*, Spektrum Akademischer Verlag, Heidelberg, 1995.
23. U. Kreibig and M. Vollmer, *Optical properties of metal clusters, Springer Series in Materials Science,* vol. 25, Springer-Verlag, Berlin, 1995.
24. J. Zhao, X. Chen and G. Wang, *Phys. Stat. Sol. (b)* **188**, 719 (1995).
25. M. Seidl, M. E. Spina and M. Brack, *Z. Phys. D* **19**, 101 (1991).
26. R. Hoffmann, *Solids and Surfaces: A Chemist's View of Bonding in Extended Structures*, VCH, New York, 1988.
27. S. Glaus, PhD thesis, University of Bern, Switzerland, in preparation.
28. W. Mönch, *Phys. Rev. B: Condens. Matter* **37**, 7129 (1988).
29. P. Junod, H. Hediger, B. Kilchör, and J. Wullschleger, *Philos. Mag.* **36**, 941 (1977).
30. S. Kitova, J. Eneva, A. Panov and H. Haefke, *J. Imaging Sci. Technol.* **38**, 484 (1994).
31. K. Kuge and N. Mii, *J. Imaging Sci. Technol.* **33**, 83 (1989).
32. J. W. Mitchell, *J. Imaging Sci. Technol.* **42**, 215 (1998).
33. E. Charlier, M. Van Doorselaer, R. Gijbels, R. De Keyzer and I. Geuens, *J. Imaging Sci. Technol.* **44**, 235 (2000).
34. T. Tani, *J. Imaging Sci. Technol.* **39**, 386 (1995).
35. R. Baetzold, *Proc. IS&T/SPSTJ's International Symposium on Silver Halide Imaging: Silver Halide in a New Millennium,* IS&T, Springfield, VA, 2000, p. 82.
36. T. Vossmeyer, L. Katsikas, M. Giersig, I. G. Popovic, K. Diesner, A. Chemseddine, A. Eychmüller, and H. Weller, *J. Phys. Chem.* **98**, 7665 (1994).
37. J. Nanda, S. Sapra, D. D. Sarma, N. Chandrasekharan, and G. Hodes, *Chem. Mater.* **12**, 1018 (2000).
38. L. Motte and M. P. Pileni, *J. Phys. Chem. B* **102**, 4104 (1998).
39. V. M. Belous, V. I. Tolstobrov, O. I. Sviridova and K. V. Chibisov, *Dokl. Phys. Chem. (Engl. Transl.)* **262**, 75 (1982).
40. K. Akamatsu, S. Takei, M. Mizuhata, A. Kajinami, S. Deki, S. Takeoka, M. Fujii, S. Hayashi, and K. Yamamoto, *Thin Solid Films* **359**, 55 (2000).
41. Y. Sun, J. E. Riggs, H. W. Rollins, and R. Guduru, *J. Phys. Chem. B* **103**, 77 (1999).
42. M. C. Brelle, J. Z. Zhang, L. Nguyen, and R. K. Mehra, *J. Phys. Chem. A* **103**, 10194 (1999).
43. R. Seifert, A. Kunzmann and G. Calzaferri, *Angew. Chem., Int. Ed. Engl.* **37**, 1521 (1998).
44. D. W. Breck, *Zeolite Molecular Sieves*, Wiley, New York, 1974.
45. M. Kawasaki, H. Hada and H. Uchida, *J. Appl. Phys.* **60**, 3945 (1986).
46. S. H. Ehrlich, *Photogr. Sci. Eng.* **23**, 348 (1979).
47. C. R. Berry, *Photogr. Sci. Eng.* **19**, 93 (1975).
48. A. Henglein, *Ber. Bunsenges. Phys. Chem.* **94**, 600 (1990).
49. W. J. Plieth, *J. Phys. Chem.* **86**, 3166 (1982).
50. J. Amblar, O. Platzer, J. Ridar, and J. Belloni, *J. Phys. Chem.* **96**, 2341 (1992).
51. J. A. Turner, J. Manassen and A. J. Nozik, *Appl. Phys. Lett.* **37**, 488 (1980).
52. M. Specht, H.-M. Kühne and J. Schefold, *Adv. Hydrogen Energy* **8**, 815 (1990).
53. O. Khaselev and J. A. Turner, *Science* **280**, 425 (1998).
54. X. Gao, S. Kocha, A. J. Frank, and J. A. Turner, *Int. J. Hydrogen Energy* **24**, 319 (1999).
55. A. J. Nozik and R. Memming, *J. Phys. Chem.* **100**, 13061 (1996).
56. H. J. Lewerenz and H. Jungblut, *Photovoltaik, Grundlagen und Anwendungen*, Springer-Verlag, Berlin, 1995, p. 252.
57. H. Tributsch, in *Solar Energy Materials*, *Structure and Bonding* vol. 49, M. J. Clarke *et al.* Eds., Springer-Verlag, Berlin, 1982, p. 137.
58. H. Gerischer, *J. Electroanal. Chem.* **82**, 133 (1977).
59. R. Memming, in *Photoelectrochemistry, Photocatalysis and Photoreactors*, M. Schiavello Ed., NATO ASI Series, Reidel Dordrecht, 1985, p.107.
60. P. Lainé, R. Seifert, R. Giovanoli, and G. Calzaferri, *New J. Chem.* **21**, 453 (1997).